SINTEF
PROCEEDINGS
2

Proceedings of the 12th International Conference on Computational Fluid Dynamics in the Oil & Gas, Metallurgical and Process Industries

Progress in Applied CFD – CFD2017

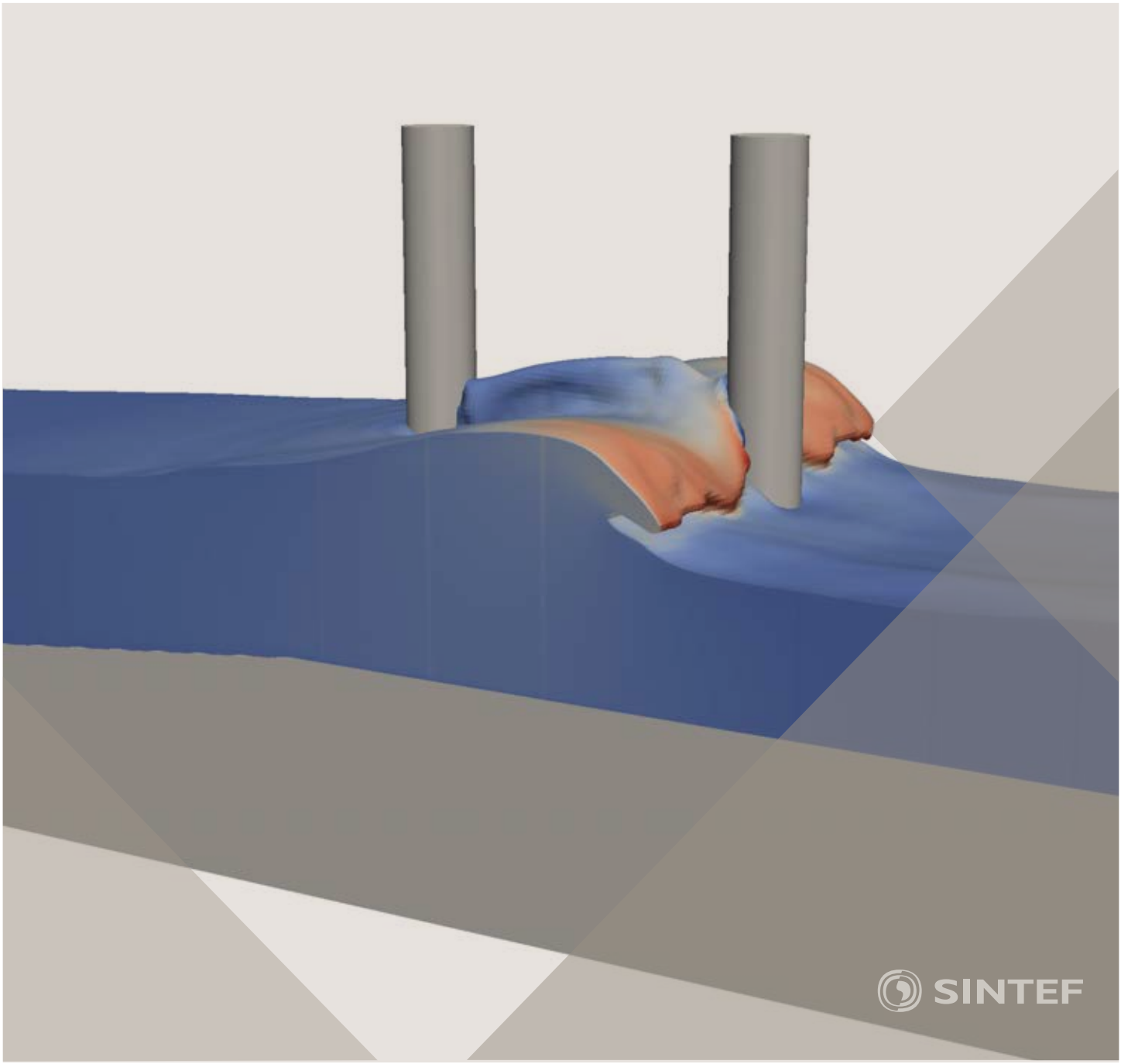

SINTEF Proceedings

Editors:
Jan Erik Olsen and Stein Tore Johansen

Progress in Applied CFD – CFD2017

Proceedings of the 12th International Conference on Computational Fluid Dynamics in the Oil & Gas, Metallurgical and Process Industries

SINTEF Academic Press

SINTEF Proceedings no 2
Editors: Jan Erik Olsen and Stein Tore Johansen
Progress in Applied CFD – CFD2017
Selected papers from 10th International Conference on Computational Fluid Dynamics in the Oil & Gas, Metallurgical and Process Industries

Key words:
CFD, Flow, Modelling

Cover, illustration: Arun Kamath

ISSN 2387-4295 (online)
ISBN 978-82-536-1544-8 (pdf)

SINTEF Academic Press
Address: Forskningsveien 3 B
PO Box 124 Blindern
N-0314 OSLO
Tel: +47 73 59 30 00
Fax: +47 22 96 55 08

www.sintef.no/byggforsk
www.sintefbok.no

SINTEF Proceedings
SINTEF Proceedings is a serial publication for peer-reviewed conference proceedings on a variety of scientific topics.
The processes of peer-reviewing of papers published in SINTEF Proceedings are administered by the conference organizers and proceedings editors. Detailed procedures will vary according to custom and practice in each scientific community.

PREFACE

This book contains all manuscripts approved by the reviewers and the organizing committee of the 12th International Conference on Computational Fluid Dynamics in the Oil & Gas, Metallurgical and Process Industries. The conference was hosted by SINTEF in Trondheim in May/June 2017 and is also known as CFD2017 for short. The conference series was initiated by CSIRO and Phil Schwarz in 1997. So far the conference has been alternating between CSIRO in Melbourne and SINTEF in Trondheim. The conferences focuses on the application of CFD in the oil and gas industries, metal production, mineral processing, power generation, chemicals and other process industries. In addition pragmatic modelling concepts and bio-mechanical applications have become an important part of the conference. The papers in this book demonstrate the current progress in applied CFD.

The conference papers undergo a review process involving two experts. Only papers accepted by the reviewers are included in the proceedings. 108 contributions were presented at the conference together with six keynote presentations. A majority of these contributions are presented by their manuscript in this collection (a few were granted to present without an accompanying manuscript).

The organizing committee would like to thank everyone who has helped with review of manuscripts, all those who helped to promote the conference and all authors who have submitted scientific contributions. We are also grateful for the support from the conference sponsors: ANSYS, SFI Metal Production and NanoSim.

Stein Tore Johansen & Jan Erik Olsen

Organizing committee:

Conference chairman: Prof. Stein Tore Johansen
Conference coordinator: Dr. Jan Erik Olsen
Dr. Bernhard Müller
Dr.Sigrid Karstad Dahl
Dr.Shahriar Amini
Dr.Ernst Meese
Dr.Josip Zoric
Dr.Jannike Solsvik
Dr.Peter Witt

Scientific committee:

Stein Tore Johansen, SINTEF/NTNU
Bernhard Müller, NTNU
Phil Schwarz, CSIRO
Akio Tomiyama, Kobe University
Hans Kuipers, Eindhoven University of Technology
Jinghai Li, Chinese Academy of Science
Markus Braun, Ansys
Simon Lo, CD-adapco
Patrick Segers, Universiteit Gent
Jiyuan Tu, RMIT
Jos Derksen, University of Aberdeen
Dmitry Eskin, Schlumberger-Doll Research
Pär Jönsson, KTH
Stefan Pirker, Johannes Kepler University
Josip Zoric, SINTEF

CONTENTS

FRONT-TRACKING SIMULATIONS OF BUBBLES RISING IN NON-NEWTONIAN FLUIDS

Alessandro BATTISTELLA[1], **Sebastian J.G. VAN SCHIJNDEL**[1], **Maike W. BALTUSSEN**[2],
Ivo ROGHAIR[1]*, **Martin VAN SINT ANNALAND**[1]

[1]Chemical Process Intensification, Department of Chemical Engineering and Chemistry, Eindhoven University of Technology, Eindhoven, the Netherlands

[2]Multi-scale Modelling of Multiphase Flows, Department of Chemical Engineering and Chemistry, Eindhoven University of Technology, Eindhoven, the Netherlands

* E-mail: i.roghair@tue.nl

ABSTRACT

In the wide and complex field of multiphase flows, bubbly flows with non-Newtonian liquids are encountered in several important applications, such as in polymer solutions or fermentation broths. Despite the widespread application of non-Newtonian liquids, most of the models and closures used in industry are valid for Newtonian fluids only, if not even restricted to air-water systems. However, it is well known that the non-Newtonian rheology significantly influences the liquid and bubble behaviour. CFD represents a great tool to study such complex systems in more detail and gain useful insights on the dynamics of gas-liquid (and possibly solid) systems with the ultimate aim to help the development or the design of industrial reactors. In this study, a DNS Front Tracking (FT) method is applied to study the rise of bubbles in different power-law fluids. Detailed information is obtained regarding the flow of single or multiple bubbles, especially concerning the viscosity profile around single rising bubbles, their shapes and their rising velocity.
To describe the bubble rise velocity in less detailed model, a closure for the drag force is needed. With the use of Front Tracking, an existing drag correlation, which was derived for Newtonian fluids, is adapted and improved to non-Newtonian rheologies. When the effect of the viscosity changes are limited, such as for not extreme exponents ($0.5 \leq n \leq 1.5$), the correlation can predict reasonably well the drag coefficient for power-law fluids.

Keywords: CFD, hydrodynamics, bubble and droplet dynamics, rheology, multiscale. .

NOMENCLATURE

Greek Symbols

$\dot{\gamma}$	Shear rate, $[s^{-1}]$
ε	Error, $[-]$
η	Apparent viscosity, [Pa s]
μ	Dynamic viscosity, [Pa s]
ρ	Mass density, $[kg\,m^{-3}]$
σ	Surface tension, $[N\,m^{-1}]$
$\boldsymbol{\tau}$	Stress tensor, $[N\,m^{-2}]$
ϕ	Volume fraction, $[-]$

Latin Symbols

A, S	Surface, [m].
C_D	Drag coefficient, $[-]$.
d	Diameter, [m].
Eö	Eötvös number Eö $= \frac{gd^2\rho}{\sigma}$, $[-]$.
$\mathbf{F}$	Force, [N].
g	Gravitational acceleration, $[m\,s^{-2}]$.
K	Power law consistency index, $[Pa\,s^n]$.
L	Half distance between plates, [m].
n	Power law index, $[-]$.
$\mathbf{n}$	Normal, $[-]$.
p	Pressure, [Pa].
Re	Reynolds number Re $= \frac{\rho u d}{\mu}$, $[-]$.
Re*	Generalized Reynolds number Re$^* = \frac{\rho u^{2-n} d^n}{K}$, $[-]$.
t	Time, [s].
$\mathbf{t}$	Tangent, $[-]$.
$\mathbf{u}$	Velocity, $[m\,s^{-1}]$.
V	Volume, $[m^3]$.

Sub/superscripts

a, b, c, i, m	Marker indicators.
G	Gas.
i	Index i.
j	Index j.
rel	Relative.
x, y	Flow directions.

INTRODUCTION

Non-Newtonian bubbly flows are widely present in nature as well as in many industrial applications, as for instance in a bioreactor (Al-Masry, 1999) where the design is crucial for the survival of microorganisms. Another well known application is polymer production, where many processes, for instance polycondensation or polymer devolatilization, involve multiphase flows with non-Newtonian fluids (Li, 1999).
An accurate description of the hydrodynamics as well as mass and heat transfer is decisive in rational the design of industrial reactors. For this reason, Computational Fluid Dynamics (CFD) represents a valuable tool to help gaining insights in the underlying physics as well as in the ultimate optimization and design. To this end, we adopted a multi-scale modelling technique (Deen *et al.*, 2004; van Sint Annaland *et al.*, 2003) where small-scale detailed models give insights for the higher, less computational expensive, scales. The latter can be summarized in two main categories: Euler-Lagrange models, where bubbles are represented by Lagrangian spheres moving in a continuum, and Euler-Euler methods where both phases are treated as a continuum. With the use of such tools, it is possible to describe small (lab) scale models up to an industrial scale reactor. However, they heavily rely on the accuracy of the used closure relations, needed to describe the interactions (drag, mass and

heat transfer) between the dispersed elements and the continous phase.

The use of direct numerical simulations (DNS) to study the smallest scale and develop such closures has been demonstrated in the past for Newtonian fluids (Dijkhuizen *et al.*, 2010a; Roghair *et al.*, 2011). Out of the many forces involved, certainly the drag force, and hence the drag coefficient, represents one of the most relevant in determining the bubble's hydrodynamic. However, despite the widespread use of non-Newtonian fluids, a complete and comprehensive description of the drag on a sphere, bubble or droplet, in such fluids (Darby and Chhabra, 2016) is still missing. In most cases, the relatively scarce information comes from experimental results and it is usually limited as a consequence of the incredibly complex variety of fluids. In numerical studies, purely viscous cases, mainly power-law fluids represent the most common type of fluids studied(Chhabra, 2006).

Ohta *et al.* (2010, 2012) developed through the years a CLSVOF model which, together with experiments, was used to study bubble shapes and velocities in different non-Newtonian fluids (both shear-thinning and shear-thickening). Radl *et al.* (2007) examined the rising of bubbles in a range of purely viscous and viscoelastic media, including mass transfer. In their work they use a hybrid front tracking/front capturing model, restricted to 2D due to the high resolution needed by the species solver. Zhang *et al.* (2010) examined the velocity and viscosity distribution, motion and bubble shape of a single bubble rising in a purely viscous shear-thinning fluid, represented by the Carreau model. For the computation, a level-set numerical approach was adopted. Some attempts have been done in the past to adapt existing drag correlations to non-Newtonian power-law fluids, such as Rodrigue (2002), which considered shear-thinning polymers at low to moderate Reynolds numbers. The proposed correlation is not suitable for high Reynolds numbers, where it does not converge to a constant as it has been well established in the recent years.

The aim of this work is to give a description of the drag coefficient in non-Newtonian fluids (both shear-thickening and shear-thinning), starting from considering single bubbles rising in power-law fluids. In the following sections, the front-tracking model used in this work will be described and verified. Then, the bubble shapes and viscosity profiles will be investigated with the numerical setup. To conclude, an outline of the drag coefficient with different power-law fluids will be given.

MODEL DESCRIPTION

The model used in this paper is a front tracking model which has been described in detail in Dijkhuizen *et al.* (2010b) and Roghair *et al.* (2015, 2016). In the following section a general description is provided, with focus on the implementation of the non-Newtonian viscosity model.

Hydrodynamics modeling

The fluid flow is described by the incompressible Navier-Stokes equation and continuity equation:

$$\rho\frac{\partial \mathbf{u}}{\partial t}+\rho\nabla\cdot(\mathbf{uu})=-\nabla p+\rho\mathbf{g}+\nabla\cdot\boldsymbol{\tau}+\mathbf{F}_\sigma \tag{1a}$$

$$\nabla\cdot\mathbf{u}=0 \tag{1b}$$

where $\mathbf{u}$ is the fluid velocity and $\mathbf{F}_\sigma$ represents a singular source-term for the surface tension at the interface. Here $\boldsymbol{\tau}$ represents the stress tensor, which becomes the very well known function of viscosity for Newtonian fluids. The velocity field is continuous even across interfaces, so a one-fluid formulation has been used. The equations are solved with a finite difference technique using a staggered discretisation (see Figure 1). The flow field is solved using a two-stage projection-correction method. After solving the momentum balance for each velocity component separately, a pressure-correction step is taken to satisfy the continuity equation. These steps use an incomplete Cholesky conjugate gradient (ICCG) method to solve the linearised equations. The boundary conditions can be adjusted between free-slip, no-slip and periodic, but only the first is used in this work. The formulation of $\boldsymbol{\tau}$ will be discussed later.

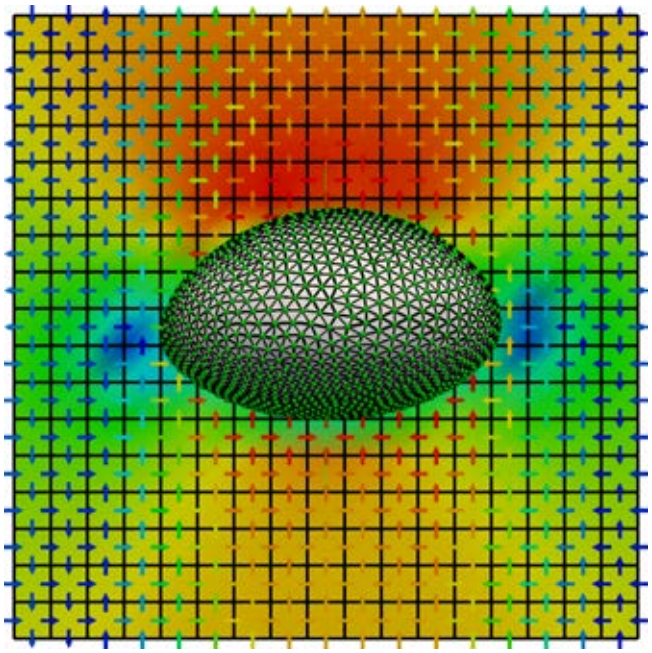

Figure 1: A zoomed snapshot of a rising FT bubble (at a very low resolution for illustration purposes), showing the tracking points and surface mesh, and the background grid with staggered velocity vectors. The colors of the background grid indicate the pressure profile, and the colors of the velocity vectors represent the magnitude.

Surface mesh

The gas-liquid interface is tracked by Lagrangian control points, which connects to a mesh composed of triangular cells, called markers (Figure 2). At every time step, after the fluid flow has been calculated, the Lagrangian control points are moved with the interpolated velocity to their new locations. The velocity is interpolated with a cubic spline method. The actual movement is performed using a 4^{th} order Runge-Kutta time stepping scheme.

Surface tension and pressure jump

$\mathbf{F}_\sigma$ is a force representing the surface tension, which can be directly calculated from the position of the interface markers. The individual pull-force of a general neighbouring marker i acting on marker m can be computed from their normal vectors and joint tangent as illustrated in Figure 2:

$$\mathbf{F}_{\sigma,i\to m}=\sigma(\mathbf{t}_{mi}\times\mathbf{n}_{mi}) \tag{2}$$

The sum of the surface forces of all markers yields the pres-

sure jump of the bubble as a whole.

$$\int_{\partial S}[p]\,dS = \int_{\partial S}\mathbf{F}_\sigma\cdot\mathbf{n}$$
$$[p] = \frac{\int_{\partial S}\mathbf{F}_\sigma\cdot\mathbf{n}}{\int_{\partial S}dS} = \frac{\sum_m \mathbf{F}_{\sigma,m}\cdot\mathbf{n}_m}{\sum_m S_m} \tag{3}$$

By distributing the total pressure jump equally back to the Eulerian mesh, the pressure jump is incorporated in the right-hand side of the momentum equations. For interfaces with a constant curvature (i.e. a sphere), the pressure jump and surface tension cancel each other out exactly, and if the curvature varies over the interface, only a relatively small net force will be transmitted to the Eulerian grid.

Phase fraction and physical properties

Since the marker positions are exactly known, the phase fraction ϕ in each Eulerian cell can be computed exactly using geometric analysis. With the phase fraction, the density of each Eulerian cell is calculated by weighted averaging. The viscosity (either Newtonian or the apparent non-Newtonian viscosity) is obtained by harmonic averaging of the kinematic viscosities (Prosperetti, 2002):

$$\rho(\mathbf{x}) = \sum_{p=0}^{n_{\text{phase}}-1}\phi_p(\mathbf{x})\,\rho_p \tag{4a}$$

$$\frac{\rho(\mathbf{x})}{\eta(\mathbf{x})} = \sum_{p=0}^{n_{\text{phase}}-1}\phi_p(\mathbf{x})\,\frac{\rho_p}{\eta_p} \tag{4b}$$

The bubble properties *i.e.* total surface area, volume and centroid position, can be efficiently obtained by summing over all triangular markers of an interface (Roghair *et al.*, 2015, 2016).

Remeshing

Due to the advection of the interface control points, the markers' geometry changes at each time step, which may lead to too large or too small triangles. This distortion affects the grid quality and can decrease the accuracy in the surface tension forces computation. Moreover, due to the discrete nature of the interface, small changes in the enclosed volume appear at every time step. Despite the small magnitude, the volume alterations can accumulate during the simulation time and must be prevented (Pivello *et al.*, 2013). The remeshing approach consists of three different parts: edge splitting and collapsing, edge swapping and smoothing. An edge is split (node addition) or collapsed (node removal) based on the edge length related to the Eulerian grid size. In some cases, it is preferable to swap an edge instead of changing the number of points: this procedure ensures that equilateral markers are preferred. Smoothing is used to enhance the quality of the grid and reduce the need for the other remeshing algorithms. The volume restoration/conservation is obtained using a method described by Kuprat *et al.* (2001). After each interface advection step and remeshing, a volume defect can be obtained by comparing the new volume with the original volume. This defect is then corrected by shifting the edges in order to restore the original volume, with particular attention on minimizing the impact on the actual geometry. A more detailed overview of the volume conservative remeshing has been presented in Roghair *et al.* (2015, 2016).

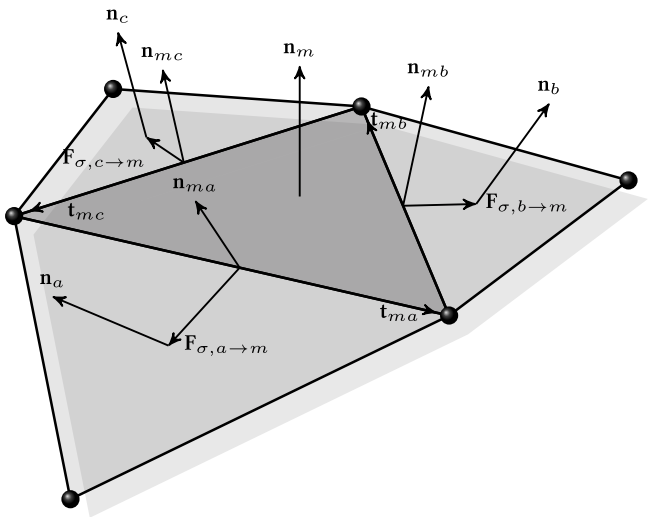

Figure 2: The surface tension calculation on marker involves the calculation of three pull-forces using the tangent and normal vectors shared with the neighbouring marker.

Viscosity model

In (inelastic) non-Newtonian fluids, the viscosity is not a constant but is a function of the strain rate. When considering a Newtonian fluid, the stress tensor $\boldsymbol{\tau}$ is given by:

$$\boldsymbol{\tau} = -\mu\left(\nabla\mathbf{u} + (\nabla\mathbf{u})^T\right) \equiv -\mu\dot{\boldsymbol{\gamma}} \tag{5}$$

in which $\dot{\boldsymbol{\gamma}}$ represents the rate of strain tensor. A commonly used model to describe a non-Newtonian fluid is the so called *generalized Newtonian model*, consisting in simply replacing the viscosity μ with an apparent viscosity η, which is a function of the shear rate (Bird *et al.*, 2007). The shear rate can be written as the magnitude of the rate of strain tensor:

$$\dot{\gamma} = \sqrt{\frac{1}{2}(\dot{\boldsymbol{\gamma}}:\dot{\boldsymbol{\gamma}})} \tag{6}$$

In this framework, the stress tensor is calculated as:

$$\boldsymbol{\tau} = -\eta\left(\nabla\mathbf{u} + (\nabla\mathbf{u})^T\right) \equiv -\eta\dot{\boldsymbol{\gamma}} \quad \text{with} \quad \eta = \eta(\dot{\gamma}) \tag{7}$$

Several empirical models are available to describe the relation between η and the shear rate, while the simplest and most widely used is the power-law model:

$$\eta = K\dot{\gamma}^{n-1} \tag{8}$$

Here K represents the consistency index while n is a constant characterizing the fluid: for $n = 1$ the relation reduces to a Newtonian fluid, for $n < 1$ the fluid is shear-thinning (viscosity reduces with the shear) and for $n > 1$ is shear-thickening (viscosity increases with the shear). This model presents a very important physical and numerical limitation, as addressed by Gabbanelli *et al.* (2005). At zero shear, the viscosity becomes infinite for a shear-thinning and zero for a shear-thickening fluid. Furthermore, it is well known that most non-Newtonian fluids do not show this behaviour in the whole range of shear rates, but rather display Newtonian plateaus around a limited non-Newtonian region, depending on the fluid rheology. More complex models have been developed to overcome this problem, such as the Carreau model, but they usually hold for a limited type of fluid (e.g. shear-thinning). A simple solution is to use a *truncated power-law* model (Gabbanelli *et al.*, 2005):

$$\eta = \eta(\dot{\gamma}) = \begin{cases} \eta_0, & \dot{\gamma} < \dot{\gamma}_0 \\ K\dot{\gamma}^{n-1}, & \dot{\gamma}_0 \leq \dot{\gamma} \leq \dot{\gamma}_\infty \\ \eta_\infty, & \dot{\gamma} > \dot{\gamma}_\infty \end{cases} \tag{9}$$

Where η_0 and η_∞ are the viscosities calculated with the respective shear rates. To keep consistency between the different cases, it has been selected to express the limits in terms of η as:

$$\begin{aligned} \eta_- &= 10^{-5}\,\mathrm{Pa\,s} \\ \eta_+ &= 10^{-1}\,\mathrm{Pa\,s} \end{aligned} \tag{10}$$

Note that in Equation 10 $+$ or $-$ represents 0 or ∞ according to the type of fluid selected *i.e.* shear-thinning or shear-thickening. Those limits have been selected in order to guarantee numerical stability especially during the first time step, while at the same time obtaining power-law fluid rheology in the whole domain for the remaining of the simulations. Preliminary calculations showed that the limits are not reached in the domain when the bubble is at pseudo steady-state. On the other hand, this implicitly assumes that the viscosity at the walls is not the bulk viscosity (η_0); this could have an influence because, due to the free slip boundary at the walls, the bulk viscosity is not η_0. Further investigation on this matter is needed, perhaps with a broader domain or different truncation limits (see Equation 9).

Verification

The front tracking model has been thoroughly validated in the past, both numerically (see Roghair *et al.* (2015)) and experimentally. For the latter, a drag correlation has been derived for single (Dijkhuizen *et al.*, 2010a) and multiple (Roghair *et al.*, 2013) bubbles rising in a initially quiescent liquid. Nonetheless, the addition of the non-Newtonian viscosity model must be verified as well. A simple test case to verify the correct implementation of the viscosity model is represented by a single phase unidirectional pressure-driven flow between two parallel plates, separated by a distance $2L$ in the direction, y, orthogonal to the flow direction, x. Since the only non-zero component of the velocity is $u_x(y)$, the Navier-Stokes equations are simplified and it is possible to obtain the stationary solution as:

$$u_x = L\frac{n}{n+1}\left(\frac{L}{K}\frac{\partial p}{\partial x}\right)^{1/n}\left(1-\left|\frac{y}{L}\right|^{\frac{n+1}{n}}\right) \tag{11}$$

From this, it is possible to calculate the flux through the rectangular domain and thus, assuming it is a constant linear profile, the inlet velocity u_{in}. With some mathematical rearrangement, one can obtain the normalized velocity profile as:

$$\frac{u_x}{u_{in}} = \frac{2n+1}{n+1}\left(1-\left|\frac{y}{L}\right|^{\frac{n+1}{n}}\right) \tag{12}$$

where y represents the distance from the center of the channel in the positive or negative directions, as it is symmetric. It is very important to notice that the simulated flow is not entirely non-Newtonian, as in the regions close to the walls there is a high shear while in the center there is zero shear at $y = 0$. This will result in three separate regions:

- a Newtonian region close to the walls
- a power-law region in between
- a Newtonian region close to the center

Since the $\dot{\gamma}$ limits are selected as broad as possible, it is possible to reduce the Newtonian regions to a very small fraction, thus assuming a power-law model in the whole domain. The simulations have been carried out with a rectangular domain where two dimensions are much larger (50 cm) than the distance between the two plates (12 mm). In the y-direction (perpendicular to the flow) a number of 100 grid nodes has been used. The two plates have a no slip boundary condition, while for the depth (the z-direction) a free slip boundary is applied. The remaining parameters are a time step of 10^{-2} s, an inlet velocity of $u_{in} = 0.01\,\mathrm{m\,s^{-1}}$ and the fluid properties are those of water (with a consistency index $K = 10^{-3}\,\mathrm{Pa\,s^n}$). A variety of different exponents has been tested, as well as a fully Newtonian case for completeness. The results of the validation are shown in Figure 3.

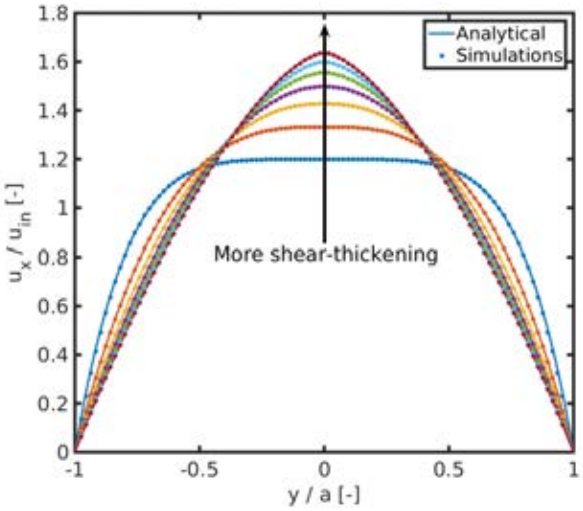

Figure 3: Comparison of simulations with the analytical solution for the steady-state velocity profiles of a 2D single phase non-Newtonian flow between parallel plates.

The simulation results match very well with the analytical solutions (see Table 1), thus confirming the validity of the power-law regime in the whole domain. The relative error has been calculated as in Equation 13 for all the cases.

$$\varepsilon_{rel} = \frac{\left\| \mathbf{u}_x - \mathbf{u}_x^{analytical} \right\|_2}{\left\| \mathbf{u}_x^{analytical} \right\|_2} \tag{13}$$

Note that the relative error here is always a positive value, while the one in the next sections is calculated without the norm to show the sign of the deviations.

Table 1: Relative error between the numerical and analytical solutions of the velocity profile for a 2D single phase non-Newtonian flow between two parallel plates.

n	ε_{rel}
0.2	0.36%
0.5	0.13%
0.8	0.11%
1	0.10%
1.2	0.10%
1.5	0.10%
1.8	0.10%

RESULTS

Numerical setup

The domain is a square box described by an Eulerian grid of $100 \times 100 \times 100$ grid nodes. An initially spherical bubble is placed in an initially quiescent liquid with its center located at 60% of the height to gain additional information regarding its wake. While the bubble rises in a free slip domain, the window shifts so that the center of the bubble is in approximately the same position throughout the simulation (Deen *et al.*, 2004).
The typical simulation uses a time step of 1×10^{-5} s and it is performed for a total of 1 s. It is well known that, especially for larger bubbles, the velocity is oscillating. To determine the drag the terminal velocity is averaged starting from 0.2 s to discard initial start-up effects. In the case of viscous liquids, or in general when viscous effects are important, it is necessary to adequately describe the far field liquid motion. This was also investigated by Dijkhuizen *et al.* (2010a) for higher viscosity liquids. Since the objective of this work is to indeed study the influence of the change in viscosity, it has been decided to opt for a less resolved bubble (10 grid cells). Further investigations are ongoing to assess the validity of this assumption and eventually to resolve the bubble motion in more detail.

Table 2: Physical properties of the air-water system.

Property	Symbol	Value
Gas density	ρ_g	$1.25\,\mathrm{kg\,m^{-3}}$
Gas viscosity	μ_g	$1.8 \times 10^{-5}\,\mathrm{Pa\,s}$
Liquid density	ρ_l	$1000\,\mathrm{kg\,m^{-3}}$
Surface tension	σ	$0.073\,\mathrm{N\,m^{-1}}$

The physical properties of the system were chosen with the aim to resemble an air-water system for the Newtonian cases (see Table 2). The liquid viscosity is of course depending on the power-law behaviour of the fluid. Simulations have been performed for different exponents as well as bubble sizes (see Table 3). One case has been selected with a higher (100 times the one of the other cases) K, to investigate more viscous regimes. For this case, also the limits have been shifted by 2 orders of magnitude while keeping the same power-law window. For all these cases simulations with $n = 0.2, 0.5, 0.8, 1, 1.2, 1.5, 1.8$ have been performed.

Table 3: Settings used in the different simulation cases.

Case	d_b [mm]	$K \times 10^{-3}$ [Pa s^n]	Eö
1	0.5	1	3.35×10^{-2}
2	2.0	1	0.54
3	4.0	1	2.15
4	4.0	100[1]	2.15

[1] *Different viscosity limits*

Viscosity profiles

As shown in the appendix, the non-Newtonian viscosity model has a large influence on bubble shape, as well as the bubble behaviour. In Figures 10, 11 and 12 in the appendix, some snapshots of the different cases are shown. As expected, in all the shear-thickening cases the bubble shape becomes more spherical as a consequence of the increased viscosity in the fluid immediately surrounding the bubble. Moreover, the bubble pattern is highly affected for the 4 mm case; the Newtonian case shows a meandering and wobbling bubble while it is rising in a straight line for the non-Newtonian cases, see also Figures 4 and 5. This is similar to a bubble rising in a more viscous fluid. The viscosity is mainly affected at the bubble front (where there is a highly shear-thickening region) and then the liquid passes the bub-

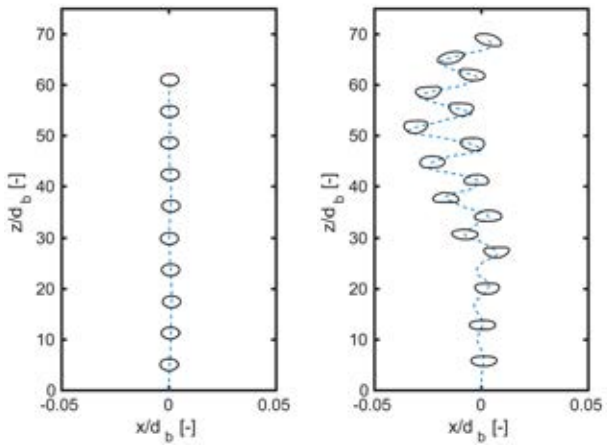

(a) $n = 1.5$ **(b)** $n = 1$

Figure 4: Comparison of the Newtonian and shear-thickening cases for a 4 mm bubble. It is possible to notice a remarkable change in shape and rising pattern, due to the viscosity alteration.

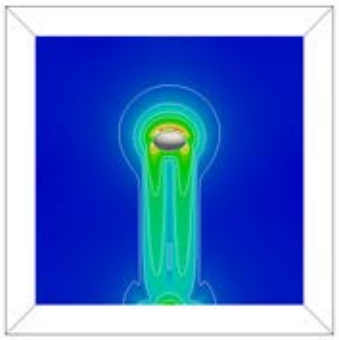

(a) $n = 1.5$

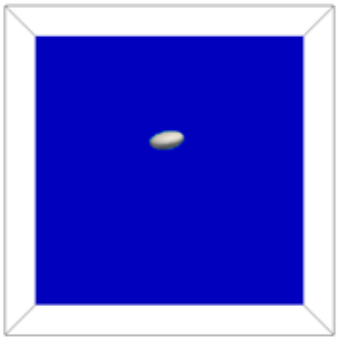

(b) $n = 1$

Figure 5: Snapshots of the viscosity profiles around a 4 mm bubble in a Newtonian and in a shear-thickening. The colors range from lower viscosity (blue) to higher viscosity (red).

ble forming a higher viscosity tail in the wake. Since the larger bubble rises faster, the viscosity reaches a higher peak in front of the bubble, while the viscosity is affected in a larger part of the domain for the smaller 0.5 mm bubble.
When inspecting the shear-thinning cases, one can observe that the shape is slightly less spherical. The meandering 4 mm bubble maintains the behaviour and this is also visible in the viscosity profile which follows the bubble pattern. In all three cases two higher viscosity regions can be observed at the walls (also observed in the past by Ohta *et al.* (2010)). Interestingly, unlike the shear-thickening case, the region with higher viscosity gradients is indeed at the walls, and mostly in the wake. In addition, again in this case the bubble rises faster for the 4 mm case, so the viscosity reaches higher (and lower) values due to higher velocity gradients. The quantification of the effects on the drag coefficient is discussed in the next sections.

Drag coefficient

The front-tracking model has been used in the past to derive a drag correlation for both single bubble (Dijkhuizen *et al.*, 2010a) and bubbles rising in a swarm (Roghair *et al.*, 2011), to be used in higher scale model such as Euler-Lagrange models. The terminal velocity of a single bubble rising in a liquid is determined by the drag that the bubble experiences. The macroscopic force balance on a bubble is given by:

$$m\frac{d\mathbf{u}}{dt} = \mathbf{F}_G + \mathbf{F}_P + \mathbf{F}_D + \mathbf{F}_L + \mathbf{F}_{VM} + \mathbf{F}_W \tag{14}$$

Out of the many forces acting on the bubble, the drag force is the most important in determining its rise velocity. Assuming that the liquid is infinite (*i.e.* zero bulk velocity), this force can be expressed as:

$$\mathbf{F}_D = -\frac{1}{8}C_D\rho_l\pi d_b^2\left|\mathbf{u}_\infty\right|^2 \tag{15}$$

When the bubble is rising in a pseudo steady-state, the drag force ($\mathbf{F}_D$) balances the buoyancy force ($\mathbf{F}_P + \mathbf{F}_G$); some mathematical rearrangement from Equation 14 neglecting the other forces leads to the well-known expression for the drag coefficient:

$$C_D = \frac{4}{3}\frac{d_b\left(\rho_l - \rho_g\right)\mathbf{g}}{\rho_l\left|\mathbf{u}_\infty\right|^2} \tag{16}$$

In many higher scale models, such as Euler-Euler or Euler-Lagrange models, the force balance on bubbles relies on the use of closure relations; for this reason it becomes unquestionably important to properly predict the drag coefficient. Many works exist in literature, starting from the drag on spherical particles (Stokes, 1851; Clift *et al.*, 1978) to arrive at the work of Tomiyama *et al.* (1998, 2002). This work is an extension to non-Newtonian fluids of the drag correlation obtained by Dijkhuizen *et al.* (2010a) and Roghair *et al.* (2011). In particular, Dijkhuizen *et al.* (2010a) described the drag coefficient as:

$$C_D = \sqrt{C_D(\mathrm{Re})^2 + C_D(\mathrm{E\ddot{o}})^2} \tag{17}$$

where the Reynolds dependent part is described as (Mei *et al.*, 1994):

$$C_D(\mathrm{Re}) = \frac{16}{\mathrm{Re}}\left(1 + \frac{2}{1 + \frac{16}{\mathrm{Re}} + \frac{3.315}{\sqrt{\mathrm{Re}}}}\right) \tag{18}$$

and the Eötvös dependent part as:

$$C_D(\mathrm{E\ddot{o}}) = \frac{4\mathrm{E\ddot{o}}}{9.5 + \mathrm{E\ddot{o}}} \tag{19}$$

It is very important to notice that, while the Eötvös number can be easily calculated, for Equation 18 the Reynolds number includes the viscosity, which is not a constant for a power-law fluid. Therefore, a generalized Reynolds number for power-law fluids has been introduced (Chhabra, 2006):

$$\mathrm{Re}^* = \frac{\rho u^{2-n} d_b^n}{K} \tag{20}$$

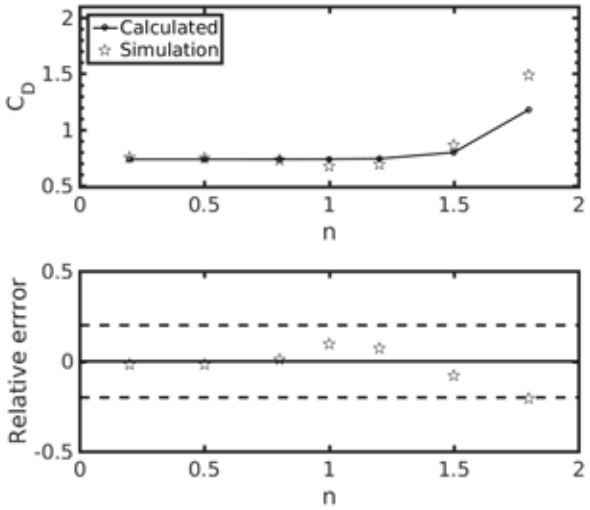

Figure 6: Drag coefficient (C_D) of a 4 mm bubble rising in different power-law fluids, with consistency index $K = 10^{-3}$ Pa s^n. The relative error is shown with ±20% error lines.

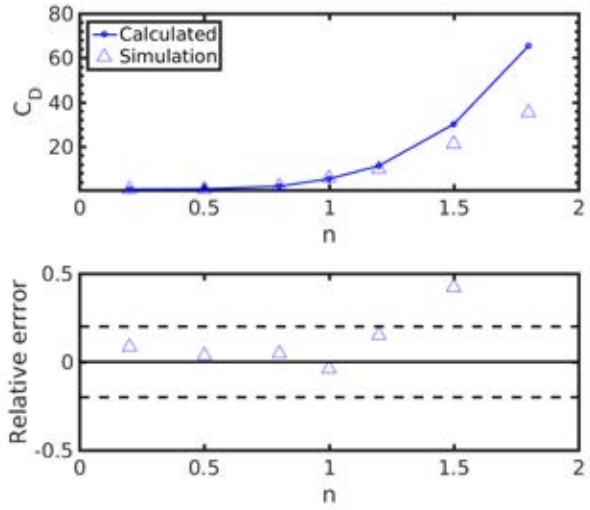

Figure 7: Drag coefficient (C_D) of a 4 mm bubble rising in different power-law fluids, with consistency index $K = 10^{-1}$ Pa s^n. The relative error is shown with ±20% error lines.

Eötvös dominant regime

The drag coefficient is determined by two different contributions: the Eötvös and the Reynolds dependent parts. At high

Eötvös numbers, such as for bigger and deformed bubbles, the $C_D(\text{Eö})$ is dominant, while the $C_D(\text{Re})$ becomes negligible. This is visible in Figure 6, showing that the total drag is constant for most of the different exponents, as a result of the high $C_D(\text{Eö})$ contribution which is constant since the Eö number is not affected by the viscosity. When the exponent becomes higher, such as for $n = 1.5$ or $n = 1.8$, the liquid is strongly shear-thickening. This affects the Re number, as the bubble is slowed down by the higher viscosity and becomes more spherical, and a considerable deviation occurs from the calculated drag coefficient. Despite this, for most of the cases the drag correlation is able to properly predict the total drag coefficient within a 20% deviation. When the consistency index K is increased by two orders of magnitude (see Figure 7), the effect of the highly shear thickening regime becomes much more pronounced with deviations up to 85%. In both cases, this deviation can be explained by considering the higher viscous contribution to the drag, which is more pronounced for the high viscosity case 4.

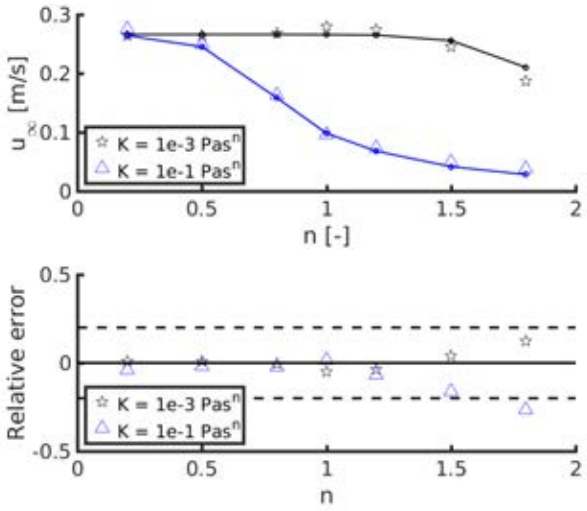

Figure 8: Terminal velocity of a 4 mm bubble rising in different power-law fluids, with two different consistency indexes. The relative error is shown with ±20% error lines.

The calculated drag coefficient has been used to determine the bubble terminal velocity (see Figure 8). The comparison with the simulation's data shows that the terminal velocity of case 3 can be reasonably well predicted for all the given exponents with a maximum relative error of 12% for the higher shear-thickening exponent, while for the other cases it is within 5%. Again, a more pronounced effect appears for case 4, where the error is within 6% for the other cases while it is 16% and 26% for the two higher exponents.
It is clear that the drag correlation of Dijkhuizen is able to predict within a reasonable accuracy the terminal velocity, until the fluid becomes vert shear-thickening ($n > 1.5$), where strong deviations occur.

Reynolds dominant regime

For smaller bubbles the Reynolds number decreases and the Reynolds dependent part of the drag starts to play a considerable role in the total drag coefficient.
A similar trend as in the previous section can be discerned from Figure 9. As soon as the exponent rises to $n = 1.5$ or higher, the drag coefficient has a drastic increase and the velocity decreases. Despite the similar behaviour, it is possible to notice how, for both bubbles, there is a clear trend in the error distribution, with many errors in the shear-thinning region outside the 50% area. This means that the correlation is not able to fully describe the drag force in this regime, which is where viscous effects are more important. Observing the bubble with $d_b = 0.5$ mm, it is clearly visible that the error is large both in the shear-thickening and in the shear-thinning regions. Moreover, also the 2 mm bubble (which is in the transition between the two regimes) shows a clear trend, with a large deviation for the most shear-thinning case.

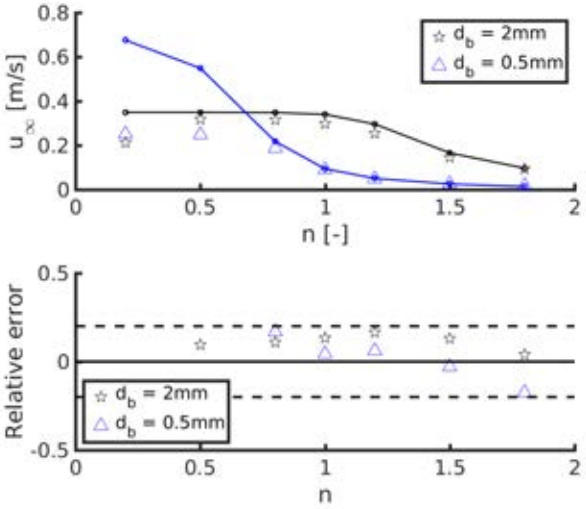

Figure 9: Terminal velocity of a 0.5mm and a 2mm bubble rising in different power-law fluids, with consistency index $K = 10^{-3}\,\text{Pa s}^n$. The relative error is shown with ±20% error lines.

In Figure 9 the terminal velocities are calculated. It is immediately visible that there is a large deviation for the 0.5 mm bubble, which reaches a plateau in the velocity for low exponents not described by the correlation. This might be due to the fact that, for extreme shear-thinning cases, the liquid viscosity approaches and even goes lower than the gas viscosity. Moreover, this could also be a consequence of an insufficient bubble or domain resolution, which needs to be farther investigated.
Despite the somewhat expected deviations from the Newtonian correlation, it is noticeable how we can predict the drag coefficient with a reasonable agreement when the exponent does not reach extreme values (e.g. within ±0.5 from 1).

CONCLUDING REMARKS

This work has shown the possibility to verify and ultimately obtain drag information for single bubbles in non-Newtonian power-law fluids using Front-Tracking simulations. The drag relation proposed by Dijkhuizen is able to reasonably well predict the drag coefficient and hence the terminal velocity for moderately non-Newtonian fluids (e.g. $0.5 \leq n \leq 1.5$) while more research has to be carried out for more extreme exponents. It is noticeable how the larger bubbles, where the Eö number is the most important in determining the drag, have in general a very good agreement with the correlation, due to the limited importance of viscous effects. On the other hand, for smaller bubbles large deviations occur from the correlation when the power-law exponent is higher (or lower). Moreover, special attention should be paid to the bubble resolution: more resolved simulations are being performed to

gain more insights. Eventually, the work will be extended to swarms of bubbles and the outcome will be used for the development of a Euler-Lagrange model in the multi-scale modelling approach.

AKNOWLEDGEMENTS

This work is part of the Industrial Partnership Programme i36 Dense Bubbly Flows that is carried out under an agreement between Akzo Nobel Chemicals International B.V., DSM Innovation Center B.V., Sabic Global Technologies B.V., Shell Global Solutions B.V., Tata Steel Nederland Technology B.V.and the Netherlands Organisation for Scientific Research (NWO).

REFERENCES

AL-MASRY, W.A. (1999). "Effect of scale-up on average shear rates for aerated non-Newtonian liquids in external loop airlift reactors." *Biotechnology and bioengineering*, **62(4)**, 494–498.

BIRD, R.B., STEWART, W.E. and LIGHTFOOT, E.N. (2007). *Transport Phenomena*. Revised 2n ed. John Wiley & Sons, New York.

CHHABRA, R.P. (2006). *Bubbles, Drops, and Particles in Non-Newtonian Fluids, Second Edition*. Chemical Industries. CRC Press.

CLIFT, R., GRACE, J.R. and WEBER, M.F. (1978). *Bubbles, Drops and Particles*. Academic Press, New York.

DARBY, R. and CHHABRA, R.P. (2016). *Chemical Engineering Fluid Mechanics, Third Edition*. CRC Press.

DEEN, N.G., VAN SINT ANNALAND, M. and KUIPERS, J.A.M. (2004). "Multi-scale modeling of dispersed gas-liquid two-phase flow". *Chem. Eng. Sci.*, **59(8-9)**, 1853–1861.

DIJKHUIZEN, W., ROGHAIR, I., VAN SINT ANNALAND, M. and KUIPERS, J.A.M. (2010a). "DNS of gas bubbles behaviour using an improved 3D front tracking model–Drag force on isolated bubbles and comparison with experiments". *Chem. Eng. Sci.*, **65(4)**, 1415–1426.

DIJKHUIZEN, W., ROGHAIR, I., VAN SINT ANNALAND, M. and KUIPERS, J.A.M. (2010b). "DNS of gas bubbles behaviour using an improved 3D front tracking model–Model development". *Chem. Eng. Sci.*, **65(4)**, 1427–1437.

GABBANELLI, S., DRAZER, G. and KOPLIK, J. (2005). "Lattice Boltzmann method for non-Newtonian (power-law) fluids". *Physical Review E - Statistical, Nonlinear, and Soft Matter Physics*, **72(4)**, 046312.

KUPRAT, A., KHAMAYSEH, A., GEORGE, D. and LARKEY, L. (2001). "Volume Conserving Smoothing for Piecewise Linear Curves, Surfaces, and Triple Lines". *J. Comp. Phys.*, **172(1)**, 99–118.

LI, H.Z. (1999). "Bubbles in non-Newtonian fluids: Formation, interactions and coalescence". *Chemical Engineering Science*, **54(13-14)**, 2247–2254.

MEI, R., KLAUSNER, J.F. and LAWRENCE, C.J. (1994). "A note on the history force on a spherical bubble at finite Reynolds number". *Phys. Fluids*, **6(1)**, 418–420.

OHTA, M., YOSHIDA, Y. and SUSSMAN, M. (2010). "A computational study of the dynamic motion of a bubble rising in Carreau model fluids". *Fluid Dynamics Research*, **42(2)**, 025501.

OHTA, M., KIMURA, S., FURUKAWA, T., YOSHIDA, Y. and SUSSMAN, M. (2012). "Numerical Simulations of a Bubble Rising through a Shear-Thickening Fluid". *Journal of Chemical Engineering of Japan*, **45(9)**, 713–720.

PIVELLO, M., VILLAR, M., SERFATY, R., ROMA, A. and SILVEIRA-NETO, A. (2013). "A fully adaptive front tracking method for the simulation of two phase flows". *International Journal of Multiphase Flow*, **58**, 72–82.

PROSPERETTI, A. (2002). "Navier-Stokes numerical algorithms for free-surface flow computations: an overview". *Drop-surface interaction*, **456**, 237–257.

RADL, S., TRYGGVASON, G. and KHINAST, J.G. (2007). "Flow and mass transfer of fully resolved bubbles in non-Newtonian fluids". *AIChE Journal*, **53(7)**, 1861–1878.

RODRIGUE, D. (2002). "A simple correlation for gas bubbles rising in power-law fluids". *The Canadian Journal of Chemical Engineering*, **80(2)**, 289–292.

ROGHAIR, I., LAU, Y.M., DEEN, N.G., SLAGTER, H.M., BALTUSSEN, M.W., VAN SINT ANNALAND, M. and KUIPERS, J.A.M. (2011). "On the drag force of bubbles in bubble swarms at intermediate and high Reynolds numbers". *Chemical Engineering Science*, **66(14)**, 3204–3211.

ROGHAIR, I., VAN SINT ANNALAND, M. and KUIPERS, J.A.M. (2016). "An improved Front-Tracking technique for the simulation of mass transfer in dense bubbly flows". *Chemical Engineering Science*, **152**, 351–369.

ROGHAIR, I., VAN SINT ANNALAND, M. and KUIPERS, J.A.M. (2013). "Drag force and clustering in bubble swarms". *AIChE Journal*, **59(5)**, 1791–1800.

ROGHAIR, I., VAN SINT ANNALAND, M. and KUIPERS, J.A.M. (2015). "An enhanced front tracking method featuring volume conservative remeshing and mass transfer". *Progress in Applied CFD*, 59–71.

STOKES, G.G. (1851). "On the Effect of the Internal Friction of Fluids on the Motion of Pendulums". *Transactions of the Cambridge Philosophical Society*, **9(part II)**, 8–106.

TOMIYAMA, A., KATAOKA, I., ZUN, I. and SAKAGUCHI, T. (1998). "Drag Coefficients of Single Bubbles under Normal and Micro Gravity Conditions." *JSME International Journal Series B*, **41(2)**, 472–479.

TOMIYAMA, A., TAMAI, H., ZUN, I. and HOSOKAWA, S. (2002). "Transverse migration of single bubbles in simple shear flows". *Chemical Engineering Science*, **57(11)**, 1849–1858.

VAN SINT ANNALAND, M., DEEN, N.G. and KUIPERS, J.A.M. (2003). *Multi-level modeling of dispersed gas-liquid two-phase flows*. Heat and mass transfer. Springer, Berlin.

ZHANG, L., YANG, C. and MAO, Z.S. (2010). "Numerical simulation of a bubble rising in shear-thinning fluids". *Journal of Non-Newtonian Fluid Mechanics*, **165(11-12)**, 555–567.

APPENDIX

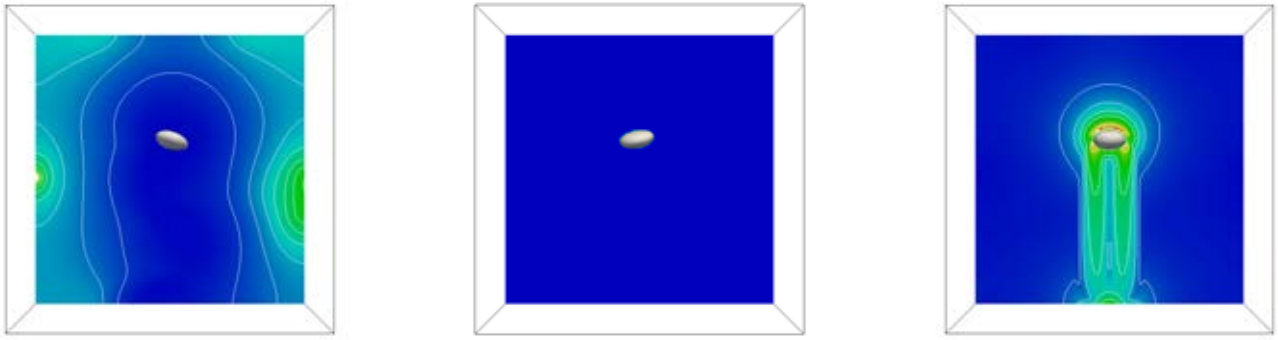

(a) $n = 0.5$ **(b)** $n = 1$ **(c)** $n = 1.5$

Figure 10: Snapshots of the viscosity profiles around a 4 mm bubble in three different fluids: (a) shear-thinning, (b) Newtonian and (c) shear-thickening. The colors range from lower viscosity (blue) to higher viscosity (red).

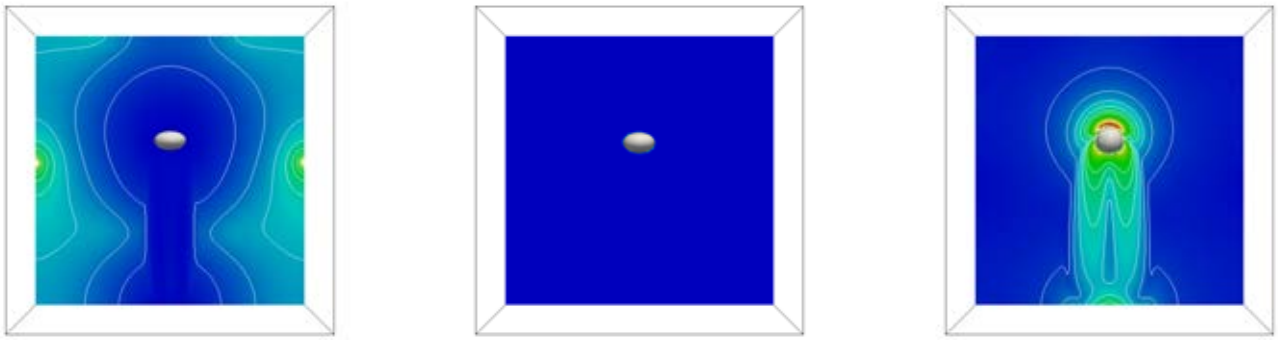

(a) $n = 0.5$ **(b)** $n = 1$ **(c)** $n = 1.5$

Figure 11: Snapshots of the viscosity profiles around a 2 mm bubble in three different fluids: (a) shear-thinning, (b) Newtonian and (c) shear-thickening. The colors range from lower viscosity (blue) to higher viscosity (red).

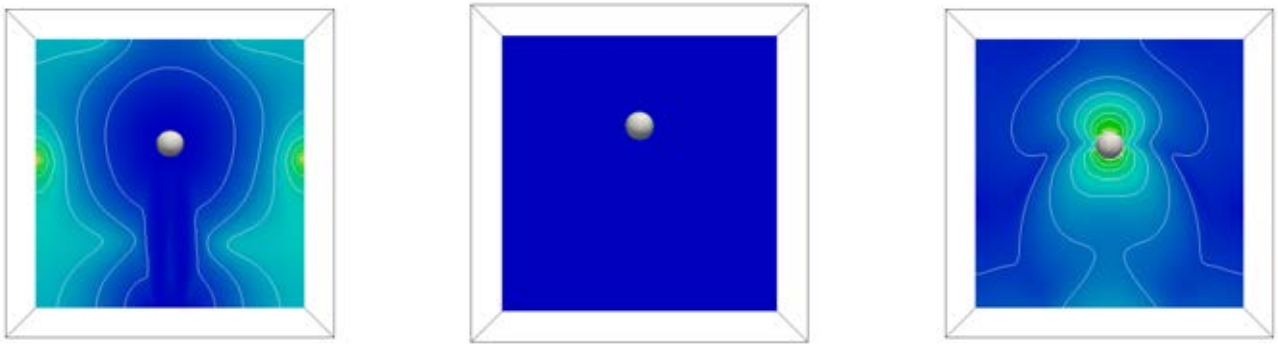

(a) $n = 0.5$ **(b)** $n = 1$ **(c)** $n = 1.5$

Figure 12: Snapshots of the viscosity profiles around a 0.5 mm bubble in three different fluids: (a) shear-thinning, (b) Newtonian and (c) shear-thickening. The colors range from lower viscosity (blue) to higher viscosity (red).